

## Full paper

# Highly stable nitrogen-doped carbon nanotubes derived from carbon dots and metal-organic frameworks toward excellent efficient electrocatalyst for oxygen reduction reaction



Wen-Jun Niu<sup>a,b,\*\*</sup>, Ya-Ping Wang<sup>a,b</sup>, Jin-Zhong He<sup>a,b</sup>, Wen-Wu Liu<sup>a,b</sup>, Mao-Cheng Liu<sup>a,b</sup>,  
Dan Shan<sup>c</sup>, Ling Lee<sup>d</sup>, Yu-Lun Chueh<sup>d,e,f,\*</sup>

<sup>a</sup> Key Laboratory of Advanced Processing and Recycling of Non-ferrous Metals, Lanzhou University of Technology, Lanzhou, 730050, PR China

<sup>b</sup> School of Materials Science and Engineering, Lanzhou University of Technology, Lanzhou, 730050, PR China

<sup>c</sup> School of Environmental and Biological Engineering, Nanjing University of Science and Technology, Nanjing, 210094, PR China

<sup>d</sup> Department of Materials Science and Engineering, National Tsing Hua University, Hsinchu, 30013, Taiwan, ROC

<sup>e</sup> Department of Physics, National Sun Yat-Sen University, Kaohsiung, 80424, Taiwan, ROC

<sup>f</sup> Frontier Research Center on Fundamental and Applied Sciences of Matters, National Tsing Hua University, Hsinchu, 30013, Taiwan, ROC

## ARTICLE INFO

## Keywords:

Nitrogen-doped carbon nanotubes

Nitrogen-doped carbon dots

Metal-organic frameworks

Electrocatalyst

Oxygen reduction reaction

## ABSTRACT

A highly efficient nitrogen-doped carbon nanotubes (N-CNTs) electrocatalyst derived from nitrogen-doped carbon dots (N-Cdots) and metal-organic frameworks (MOFs) for oxygen reduction reaction (ORR) was demonstrated successfully for the first time. The N-Cdots with plenty of hydroxyl and amine groups can favor the formation of N-CNTs through the catalytic decomposition of MOFs in a lower temperature. On the other hand, the N-Cdots serve as inducers of the graphitic structure and supply extra nitrogen, extending a potential electrocatalytic activity of N-CNTs. Results show that the N-CNTs provided an excellent ORR electrocatalytic performance, yielding a positive onset potential of 0.88 V vs. RHE and a high kinetic current density of up to  $5.58 \text{ mA cm}^{-2}$  at 0.2 V. In addition, the slope of N-CNTs being  $\sim 81 \text{ mV/dec}$  can be found to be much lower than that of the Pt/C catalyst ( $\sim 132 \text{ mV/dec}$ ). These superior performances are attributed to defects in the graphitic crystal structure and the synergistic coupling effects of N-Cdots and N-CNTs. In addition, a slight loss in activity for the N-CNTs catalyst can be found whereas the Pt/C catalyst decreases nearly 45% of its initial activity, which exhibit highly catalytic durability and tolerance to methanol in an alkaline media.

## 1. Introduction

Rechargeable devices, such as fuel cells and metal-air batteries, have been the focus of considerable amount of researches in recent years as they can offer a high energy conversion efficiency and are environmentally friendly [1–5]. However, the sluggish kinetics of the oxygen reduction reaction (ORR) at the cathode in rechargeable devices hinders their further development. Although platinum-loaded carbon (Pt/C) is currently the most efficient electrocatalyst for the ORR [6,7], its widespread commercialization is hampered by its extremely limited content in the earth, poor stability and inactivation with respect to methanol poisoning [8,9]. It is thus imperative to develop low-cost and highly active ORR electrocatalysts for use in future rechargeable devices.

It has been proven that N-CNTs provide an extremely effective electrocatalytic ORR performance and are highly stable compared to commercially available Pt/C [10,11]. Recent intensive research has focused on arc-discharge, laser-ablation and chemical vapor deposition (CVD) methods to synthesize N-CNTs in the presence of  $\text{NH}_3$ ,  $\text{HNO}_3$  and pyridine among others [12–16]. However, harsh synthetic conditions and high energy dissipation have been shown to limit the further application of those nitrogen-doped carbon nanomaterials. In addition, the strategy involved in their large-scale syntheses is complex. It is thus necessary to urgently develop a simple and cost-effective way of preparing N-CNTs that have excellent ORR electrocatalytic activity. On the other hand, MOFs are a new kind of porous coordination compound that is comprised of metal ions or clusters and coordinate with organic ligands. They have a rich carbon and nitrogen content and have been

\* Corresponding author. Department of Materials Science and Engineering, National Tsing Hua University, Hsinchu, 30013, Taiwan, ROC.

\*\* Corresponding author. Key Laboratory of Advanced Processing and Recycling of Non-ferrous Metals, Lanzhou University of Technology, Lanzhou, 730050, PR China.

E-mail addresses: [niuwenjun0509@163.com](mailto:niuwenjun0509@163.com) (W.-J. Niu), [ylchueh@mx.nthu.edu.tw](mailto:ylchueh@mx.nthu.edu.tw) (Y.-L. Chueh).

<https://doi.org/10.1016/j.nanoen.2019.05.074>

Received 31 March 2019; Received in revised form 18 May 2019; Accepted 29 May 2019

Available online 30 May 2019

2211-2855/ © 2019 Published by Elsevier Ltd.

identified as promising precursors for synthesizing N-CNTs. For example, Yang et al. reported the synthesis of N-CNTs via the direct solid pyrolysis of Zn-Fe-ZIF, with which catalytically active  $\text{Fe}^{2+}$  can be incorporated in an  $\text{N}_2$  atmosphere [17]. Lou et al. has reported the preparation of N-CNTs at high temperature pyrolysis ZIFs in the presence of  $\text{H}_2$  [18]. Furthermore, Mai et al. found that the generated reducing gases ( $\text{NH}_3$  and  $\text{H}_2$ ) turned metal ions/clusters into metal nanocatalysts during the pyrolysis process, which then further catalyzed the residual organic units to form CNTs [19]. Therefore, the high pyrolysis temperature, inevitable aggregation, low content of nitrogen doping and low degree of graphitization continue to impede their further application, leading to synthesizing N-CNTs from MOFs at a low-temperature by a general method remaining a formidable challenge.

N-Cdots are a newly emerging carbon nanomaterial, which has been attracted enormous attention because of its excellent ORR electrocatalytic activity [20–23]. It has also been proven that the nitrogen-doping is a powerful approach used to change the charge and spin density of Cdots, providing an effective way of extending its potential electrocatalytic activity toward ORR [24–27]. Moreover, studies have found that N-Cdots can be employed as reducing agents to synthesize silver nanoparticles [28–30], which can be used in the place of other reducing gases ( $\text{NH}_3$  and  $\text{H}_2$ ) in the MOFs pyrolysis process. It can thus be extremely interesting to prepare N-CNTs via pyrolyzing a mixture of ZIFs-67 and N-Cdots because N-Cdots can induce the graphitic structure, acting as an extra nitrogen supplier and also favor the formation of N-CNTs through the catalytic decomposition of MOFs. In this regard, we report the preparation of N-CNTs derived from N-Cdots and MOFs via the direct pyrolysis of ZIF-67 and N-Cdots mixture in a lower temperature. The possible formation mechanism of the N-CNTs was accurately investigated by turning the pyrolysis intervals as well as mass ratio of ZIF-67 and N-Cdots mixture. The ZIF-67, in combination with N-Cdots generated synergistic effect during the pyrolysis and carbonization processes, exhibited a highly efficient ORR electrocatalytic activity and durability than commercially available Pt/C in alkaline solution. Consequently, the current works not only provide a new insight into the preparation of N-CNTs but also offer prospects in developing highly active ORR electrocatalysts in the future rechargeable devices.

## 2. Material and methods

### 2.1. Reagents and materials

Alanine, histidine, cobalt nitrate hexahydrate ( $\text{Co}(\text{NO}_3)_2 \cdot 6\text{H}_2\text{O}$ ), and 2-methylimidazole were purchased from J&K Scientific Inc. (Shanghai, China). A commercially available platinum-loaded carbon catalyst (Pt/C, 20 wt% Pt loading on carbon black, Johnson Matthey) was used as received. All other reagents were of analytical grade and used without further purification. Ultrapure water was prepared by the Millipore Milli-QTM system and employed throughout the following experiments.

### 2.2. Preparation of ZIF-67

ZIF-67 was prepared using a previous procedure that was slightly modified [31], where 0.45 g cobalt nitrate hexahydrate ( $\text{Co}(\text{NO}_3)_2 \cdot 6\text{H}_2\text{O}$ ) was dissolved into 3.0 mL of methanol, and 5.5 g 2-methylimidazole in 20.0 mL of methanol was then added prior to vigorous stirring for 6 h at room temperature. The resulting purple precipitates were collected by centrifuging, washed with methanol and ultrapure water in sequence at least three times, and finally dried in vacuum at 50 °C overnight. Prior to use, the ZIF-67 powder was further activated at 100 °C under vacuum for 24 h.

### 2.3. Preparation of N-CNTs

The N-Cdots were prepared using a modified protocol previously reported by us [32]. The N-CNTs were synthesized using a pyrolysis and carbonization method that involved the following procedure: 0.1 g of ZIF-67 powder was added to a 5.0 mL 1.0 mg/mL N-Cdots solution, the mixture was then placed in an alumina crucible with a cover and heated to 600 °C at a rate of 0.5 °C/min in a muffle furnace and maintained at this temperature for 4 h in a nitrogen atmosphere. The resultant powder was cooled to room temperature, washed with ultrapure water, collected by filtration and finally dried at room temperature. To enable a comparison, the synthesized ZIF-67 powder was subsequently treated solely under the same other conditions, resulting in cobalt nitrogen carbon (Co–N–C) nanohybrids. Furthermore, to gain a good understanding of the possible formation mechanism of N-CNTs, the reaction conditions, such as the mass ratio of reactants and pyrolysis intervals, were systematically determined.

### 2.4. Structural characterizations

The morphology, size and microstructure of N-Cdots, ZIF-67, and N-CNTs were analyzed by a field emission scanning electron microscopy (S-4800 FE-SEM, Hitachi, Japan) and a high-resolution transmission electron microscope (TECNAI-12 HR-TEM, Philips, Netherlands). The crystalline structure and chemical composition of N-CNTs were investigated by K-Alpha X-ray photoelectron spectroscopy (XPS, Thermo Fisher Scientific). Raman spectra were recorded on an iHR550 Raman microscope (HORIBA scientific) with 532 nm solid laser as an excitation source.

### 2.5. Electrochemical measurements

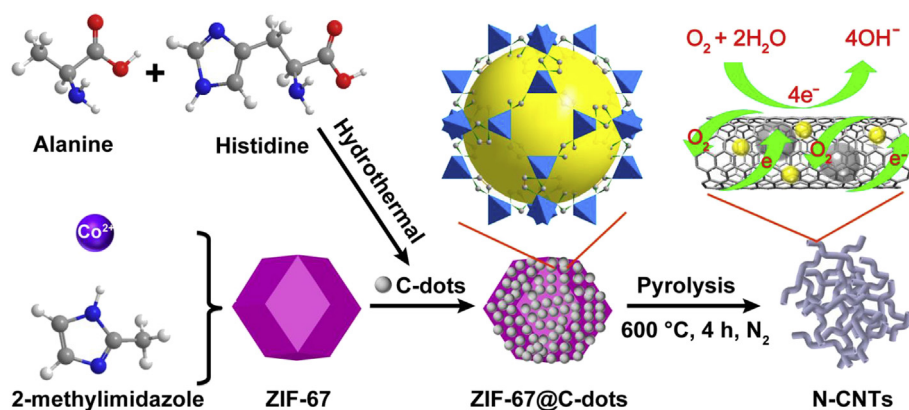
A CHI 660D electrochemical workstation (CH Instrument) was used to make cyclic voltammetry (CV) and linear sweep voltammograms (LSVs) measurements. All electrochemical studies were conducted using a conventional three electrode system, and a flow of  $\text{N}_2$  or  $\text{O}_2$  was maintained during the measurements to ensure an  $\text{N}_2$  or  $\text{O}_2$  saturated electrolyte, and an Ag/AgCl (3 M KCl) and a Pt wire were used as the reference and counter electrodes, respectively. All the potentials mentioned below are relative to the reversible hydrogen electrode (RHE) by adding a value of  $(0.197 + 0.059 \times \text{pH})$  V. A glassy carbon electrode (GCE, diameter: 3 mm) or a rotating disk electrode (RDE, Area: 0.196  $\text{cm}^2$ ) was polished carefully with 0.3 mm and 0.05 mm alumina powders on the silk. A catalyst aqueous solution of 20  $\mu\text{L}$  (10.0 mg/mL, with 5 wt % Nafion solution) was then transferred onto the electrode via a controlled drop-casting approach, and the electrode was then dried air for 12 h to serve as a working electrode. The ORR kinetics were analyzed by Koutechy–Levich plot ( $K$ – $L$ ) equation and the electron transfer number ( $n$ ) of the electrocatalyst can be derived from it:

$$\frac{1}{j} = \frac{1}{j_L} + \frac{1}{j_K} = \frac{1}{B\omega^{1/2}} + \frac{1}{j_K} \quad (1)$$

in which,  $j$  is the current density at the applied voltage,  $j_K$  is the kinetic current density,  $j_L$  is the limiting diffusion currents density, and  $\omega$  is the electrode rotating rate (rpm). The parameter  $B$  at different applied voltages could be obtained from the slope of  $K$ – $L$  plots. Meanwhile,  $n$  values at different voltages have a relationship with parameter  $B$  according to the Levich equation as below in the alkaline solution:

$$B = 0.2nF(D_{\text{O}_2})^{2/3}\nu^{-1/6}C_{\text{O}_2} \quad (2)$$

where  $n$  represents the overall transferred electron number per oxygen molecule,  $F$  is the Faraday constant with the value of  $96485 \text{ C mol}^{-1}$ ,  $D_{\text{O}_2}$  is the diffusion coefficient of  $\text{O}_2$  in 0.1 M KOH ( $1.9 \times 10^{-5} \text{ cm}^2 \text{ s}^{-1}$ ),  $\nu$  is the kinetic viscosity of the solution ( $0.01 \text{ cm}^2 \text{ s}^{-1}$ ), and  $C_{\text{O}_2}$  is the bulk concentration of  $\text{O}_2$



**Scheme 1.** Schematic illustration of highly efficient nitrogen-doped carbon nanotubes electrocatalyst derived from carbon dots and metal-organic frameworks for ORR.

( $1.2 \times 10^{-6} \text{ mol cm}^{-3}$ ). The constant 0.2 is adopted when the rotation speed is expressed in rpm in alkaline solution.

### 3. Results and discussion

Scheme 1 shows a schematic of N-CNTs derived from N-Cdots and MOFs toward highly efficient electrocatalyst of ORR. First, the N-Cdots were prepared using a modified hydrothermal carbonization protocol and a representative TEM image is shown in Fig. S1 (Supporting Information). The as-synthesized N-Cdots have a dispersive quasi-spherical shape with an average size of approximately 10 nm (Fig. S1A), and the lattice spacing of 0.304 nm agrees well with the spacing between graphite (002) layers, revealing a high-crystalline graphitic structure (Fig. S1B) [32]. The well-dispersed ZIF-67 nanocrystals exhibiting a dodecahedral appearance with an average size of approximately 300 nm were synthesized by the room-temperature reaction of  $\text{Co}(\text{NO}_3)_2$  and 2-methylimidazole in a methanol solution (Fig. S2, Supporting Information).

N-CNTs were synthesized by the simultaneous direct pyrolysis of mixed ZIF-67 and N-Cdots in an  $\text{N}_2$  atmosphere at a lower temperature, with which the morphology, size and microstructure of the N-CNTs were characterized by FE-SEM and HR-TEM as shown in Fig. 1. In Fig. 1(A), ZIF-67 precursors were formed into uniform rod-like particles with open end. Specifically, similar to the bottom-up organic method [15,16], it is apparent from the larger particles, which have a rough appearance where the ZIF-67 dodecahedron was eventually converted into thin N-CNTs with the presence of N-Cdots by the pyrolysis process. The as-prepared N-CNTs have an average diameter of approximately 15 nm as shown in Fig. 1(B). Fig. 1(C) and 1(E) show HR-TEM images of detailed structural information and the atomic lattice fringes of the N-CNTs. The HR-TEM image of the corresponding selected area shows the clear atomic lattice fringes of N-Cdots and Co nanoparticles (Fig. 1(C)). It is interesting to observe that the lattice fringes of the N-CNT are not perfectly identical to those of commercially available CNTs, which may be attributed to nitrogen doping and the catalysis of N-Cdots, an effective way of changing the charge and spin density of carbon atoms in CNTs. In addition, small domains of defective graphitic structures in the N-CNTs can be found, which are beneficial for enhancing the electrocatalytic properties of the catalyst. Note that the lattice spacing ( $\sim 0.311 \text{ nm}$ ) is coincident with the interlayer spacings of the graphite (002) as shown in Fig. 1(D) [32], while the lattice spacing ( $\sim 0.205 \text{ nm}$ ) is also consistent with the Co (111) facet as shown in Fig. 1(E) [19]. Furthermore, the energy dispersive X-ray spectroscopy (EDS) elemental mapping images of the N-CNTs (Fig. 1(F)) clearly identifies the full and uniform distribution of C, Co and N, respectively. All these results reflect the N-Cdots and MOFs are well-hybridized into the graphitic carbon structure of N-CNTs.

X-ray photoelectron spectra (XPS) were further conducted to analyze elemental compositions and nitrogen bonding configurations of N-CNTs. As expected, the survey spectrum of N-CNTs (curve b) as illustrated in Fig. 2(A) exhibits four peaks corresponding to C, O, N and Co elements where the relative elemental contents can be calculated to 76.1% for C, 11.7% for O, 10.7% for N and 1.5% for Co, respectively. To enable a comparison, the synthesized ZIF-67 powder was subsequently treated solely under the same condition, resulting in cobalt nitrogen carbon (Co-N-C) nanohybrids. As displayed in curve a of Fig. 2(A), the relative elemental compositions of Co-N-C nanohybrids can be calculated to 79.4% for C, 10.3% for O, 8.4% for N and 1.9% for Co, indicating that N-Cdots introduce not only a large number of nitrogen-containing groups but also a certain number of oxygenated functional groups on N-CNTs. The greatly increased N contents in the XPS spectrum of N-CNTs further confirms that N-Cdots are embedded into the graphitic structure. To comprehensively study the chemical/electronic environments of neighboring atoms and reveal the potential electrocatalytic activities, high resolution spectra of  $\text{C}_{1s}$ ,  $\text{N}_{1s}$  and  $\text{Co}_{2p}$  were then respectively evaluated. The  $\text{C}_{1s}$  spectrum of N-CNTs (Curve b in Fig. 2(B)) can be deconvoluted into four different bands that correspond to C-C (282.6 eV), C-N (283.6 eV), C=N/C=O (284.9 eV) and O-C=O (288.6 eV) functional groups. The slightly decreased binding energy of C-C for N-CNTs compared to the pristine Co-N-C nanohybrids (Curve a in Fig. 2(B)) can be ascribed to the incorporation of N. In contrast to the slightly increased binding energy of pyridinic N and a little decreased graphitic N in the  $\text{N}_{1s}$  spectrum of Co-N-C nanohybrids (Curve a in Fig. 2(C)), the N-CNTs (Curve b in Fig. 2(C)) exhibit four relative nitrogen species, including pyridinic N (396.8 eV), pyrrolic N (398.8 eV), graphitic N (400.3 eV) and oxidized N (404.2 eV), respectively. The results strongly confirm that the N-Cdots have been successfully doped into the N-CNTs. The graphitic N is known to be susceptible to oxygen adsorption, even at low pressures while the pyridinic N is of great importance to enhance the electrocatalytic performance for ORR [33–36]. This is why the prepared nanomaterials exhibit remarkable ORR electrocatalytic activities and details will be discussed later. Furthermore, The Co 2p XPS spectrum of the N-CNTs (Curve b in Fig. 2(D)) is composed of two noticeable peaks of Co  $2p_{1/2}$  and Co  $2p_{3/2}$ , which further split into four subpeaks assigned to  $\text{Co}^{2+}$  (779.2 and 795.3 eV) and  $\text{Co}^{3+}$  (777.3 and 793.1 eV). The slightly decreased binding energies of  $\text{Co}^{2+}$  and  $\text{Co}^{3+}$  in the N-CNTs compared to the pristine Co-N-C nanohybrids (779.4 and 795.6 eV for  $\text{Co}^{2+}$ , 777.9 and 793.3 eV for  $\text{Co}^{3+}$ ) (curve a in Fig. 2(D)) can be attributed to the incorporation of N-Cdots, which allow more Co- $\text{N}_x$  active sites to be generated, leading to an effective way of extending their potential electrocatalytic activity toward ORR [17–19].

It is well known that Raman spectroscopy is an efficient and non-destructive way of investigating the structural defects of carbon



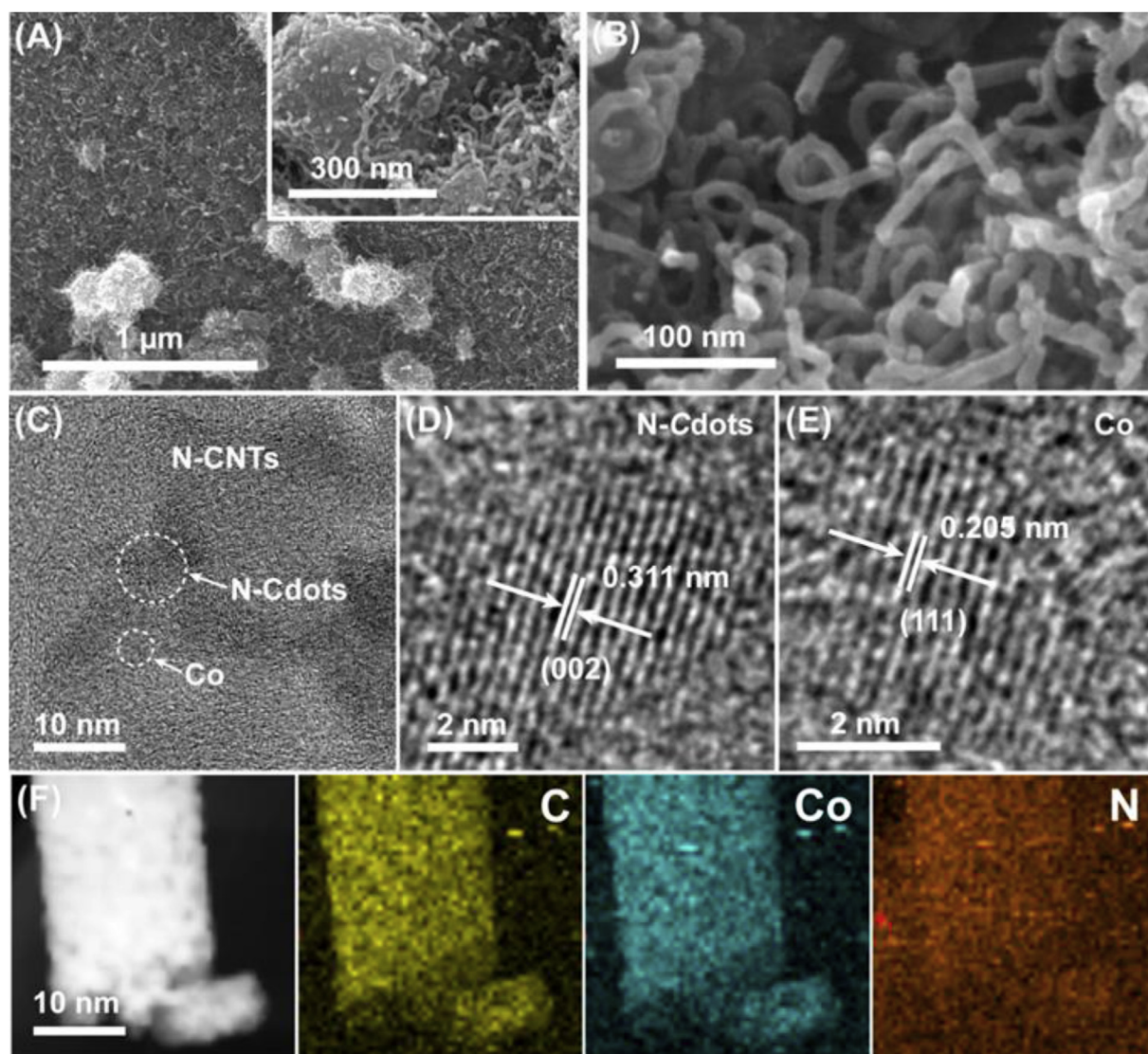


**Fig. 1.** Low-resolution (A), high-resolution (B) SEM images, high-resolution (C, D, E) TEM images and (F) Elemental mapping images of as-synthesized N-CNTs, including C, Co and N elements.

materials [37,38]. Therefore, the Co–N–C nanohybrids and N-CNTs were characterized by Raman spectroscopy using a 532 nm solid laser as an excitation source as shown in Fig. 3(A). Clearly, both samples reveal D and G peaks, which are the result of in-plane and out-plane  $sp^2$  hybridized vibration modes of carbon atoms where the difference in positions of peaks is attributed to the presence of structural defects. Furthermore, the integral intensity ratio of two peaks ( $I_D/I_G$ ) reflects the degree of defects [39–41]. As depicted in Fig. 3(A), the  $I_D/I_G = 0.845$  of the N-CNTs (curve b) is slightly smaller than that of the Co–N–C nanohybrids ( $I_D/I_G = 1.08$ , curve a), which indicates that the partial out-plane vibrations of Co–N–C nanohybrids ( $sp^3$  bonds) are converted into in-plane vibrations ( $sp^2$  bonds) in relation to N-Cdots doped at high temperature where small domains of defective graphitic structures are formed with the significantly enhanced conductivity. The reason can be explained where N-Cdots serve as both an inducer of the graphitic structure and an extra nitrogen supplier for the N-doping, which extends the potential electrocatalytic activity of the N-CNTs. As a result, as-prepared N-CNTs present excellent electrocatalytic properties that are superior to those of N-Cdots and Co–N–C nanohybrids. It has recently been discovered that the distinctive nanostructure of N-Cdots incorporated into graphene layers favors the reactivity of neighborly linked carbon atoms via alteration of electronic structure, resulting in

an excellent electrocatalytic activity [27]. It has also been found that the partially converted  $sp^2$ -hybridized carbon with small domains of defective graphitic structures formed in nitrogen-doped carbon nanomaterials can be beneficial to enhance electrocatalytic properties [26,29]. As previously mentioned, the N-Cdots can be used in place of reducing gases ( $NH_3$  and  $H_2$ ) and can favor the formation of N-CNTs through the catalytic decomposition of MOFs. Therefore, the introduction of N-Cdots strongly influences decomposition of the ZIF-67 precursors. To better understand the formation mechanism of N-CNTs, changes in crystallographic structure after the pyrolysis process were confirmed by XRD results. As can be seen in Fig. 3(B), all carbon materials exhibit a broad peak located at approximately  $24^\circ$ , belonging to the (002) interlayer peak of graphitic carbon in stark contrast to a broad peak centered at approximately  $25^\circ$  for N-Cdots (Fig. S3A, Supporting Information) and strong peaks of ZIF-67 precursor as the simulated patterns (Fig. S3B). Moreover, two weak peaks located at around  $44^\circ$  and  $52^\circ$  are assignable to the (111) and (200) diffractions of fcc Co (JPCDS file no. 15–0806) originated from the Co NPs embedded in N-CNTs as the mass ratios increase, suggesting the complete transition of N-Cdots and ZIF-67 to N-CNTs.

Furthermore, SEM images of mixed ZIF-67 and N-Cdots after the pyrolysis with different mass ratios were obtained under the same

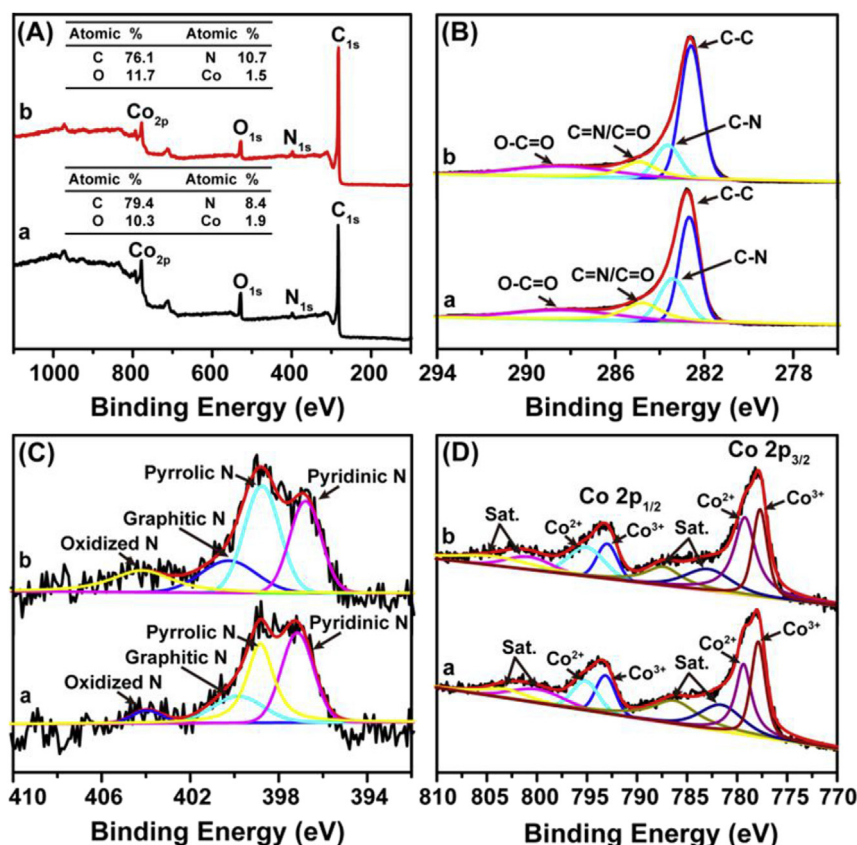


Fig. 2. (A) XPS survey spectrum, high-resolution (B)  $C_{1s}$ , (C)  $N_{1s}$  and (D)  $Co_{2p}$  peaks of Co-C-N nanohybrids (a) and N-CNTs (b), respectively.

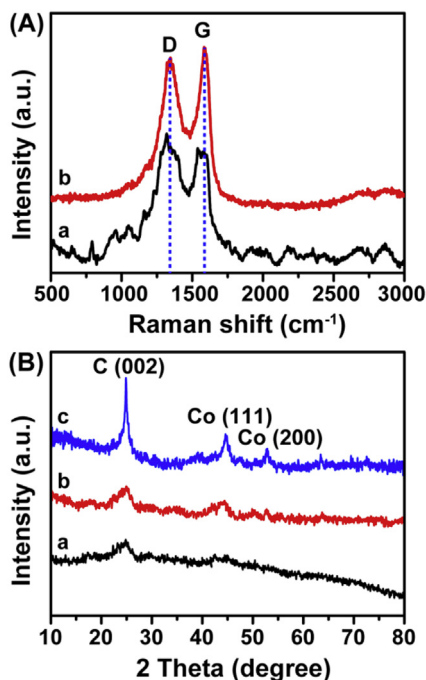
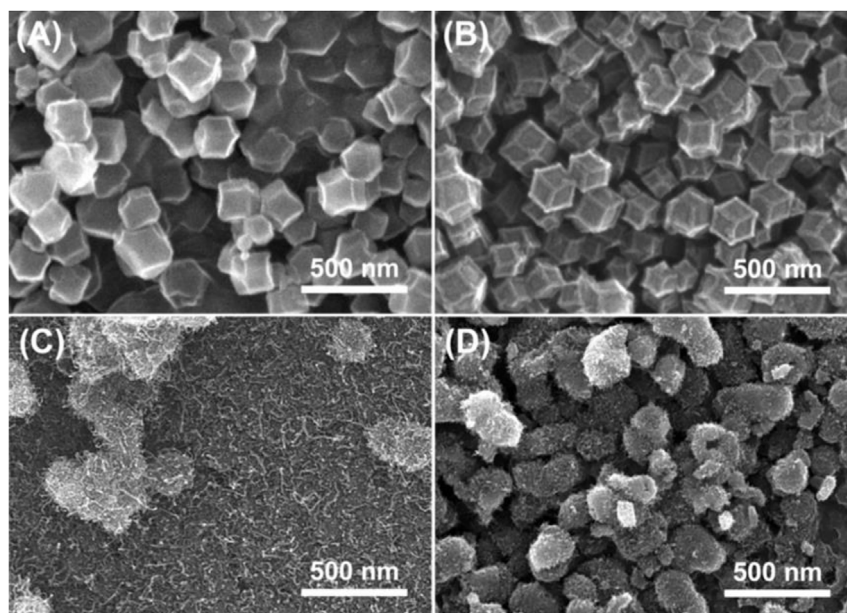


Fig. 3. (A) Raman spectra of as-prepared (a) Co-N-C nanohybrids and (b) N-CNTs. (B) XRD patterns after pyrolysis the mixed ZIF-67 and N-Cdots with different mass ratios of 10:1 (a), 20:1 (b), and 30:1 (c).

conditions. As can be seen in Fig. 4(A), the products maintained the dodecahedral morphology and no carbon nanotubes were obtained in the separated pyrolysis processes. However, when the N-Cdots were introduced and the mass ratio of ZIF-67 and N-Cdots was controlled to

30:1, the products were morphology-preserved, but the smooth surfaces become rough (Fig. 4(B)). When the concentration of N-Cdots slightly increases to 20:1, the pyrolysis is more complete and rod-like particles were formed as shown in Fig. 4(C). To the closer observation, a numbers of rod-like particles were found to grow up from surfaces of ZIF-67 precursors, for which the growth direction is considered to be from inside to outside. This explicitly suggests that ZIF-67 precursors were completed transformed into uniform N-CNTs. Nevertheless, when the concentration of N-Cdots further increases, most of ZIF-67 precursors were decomposed into irregularly shaped nanoparticles with particle sizes that were much smaller than those of precursors and some nanotubes were scattered among the particles as shown in Fig. 4(D). Moreover, the mixture of ZIF-67 and N-Cdots (mass ratio is 20:1) was pyrolyzed at 600 °C with different intervals to accurately understand the formation mechanism of N-CNTs. As can be shown in Fig. 5(A) when the sample was pyrolyzed at 600 °C for 1 h, the structures retained the dodecahedral morphology of the precursors and had a smooth interface. A large number of ZIF-67 precursors maintained the dodecahedral morphology as the pyrolysis interval was increased to 2 h (Fig. 5(B)). However, the surfaces were much rougher, which implies that only a small amount of ZIF-67 precursors were decomposed to rod-like particles. When the synthesis temperature is continuously elevated, the increased pyrolysis enables formation of a small quantity of rod-like particles and the surface of the particles becomes rougher as shown in Fig. 5(C). This is mainly attributed to incomplete pyrolysis of ZIFs-67 and insufficient growth of CNTs. As shown in Fig. 5(D), although there are still many particles with the similar size of ZIF-67, the ZIF-67 precursors attained a large quantity of uniform tubular morphology with diameters of approximately 15 nm and lengths of 300 nm after the pyrolysis interval rises to 4 h. These results are in consistency with the schematic of the stepwise thermal decomposition to form N-CNTs (Fig. 5(E)). The N-Cdots can reduce metal ions into metals, facilitating the nucleation of nanocatalysts, firstly. Then, organic residuals acting as





**Fig. 4.** SEM images of (A) pyrolysis ZIF-67 and mixed ZIF-67 and N-Cdots with different mass ratios of (B) 30:1, (C) 20:1, and (D) 10:1 at 600 °C for 4 h in an N<sub>2</sub> atmosphere, respectively.

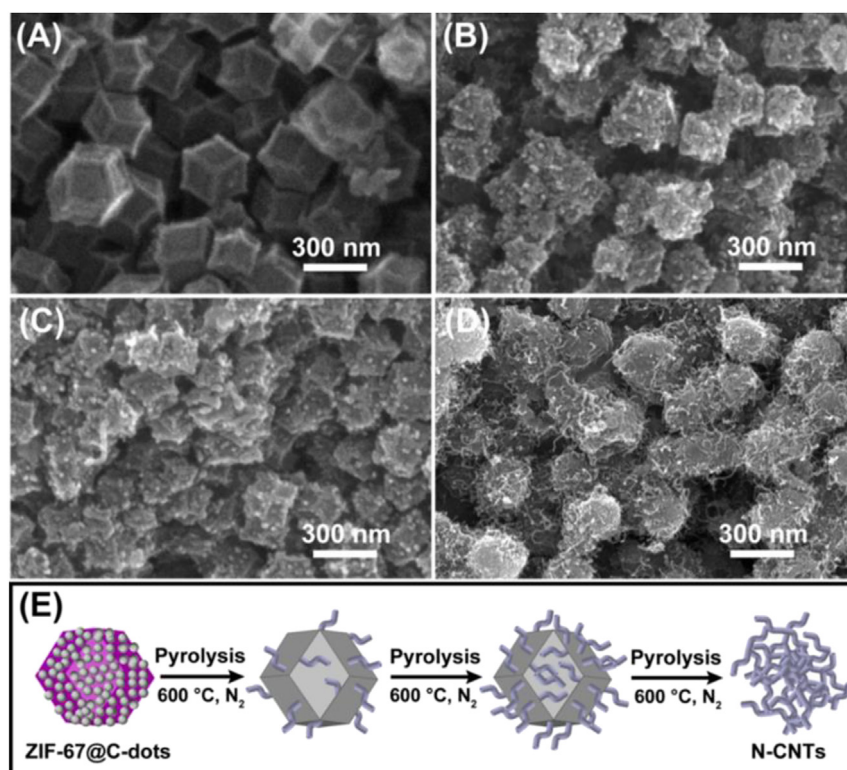


**Fig. 5.** SEM images of ZIF-67 and N-Cdots mixture (mass ratio 20:1) with different pyrolysis intervals (A) 1 h, (B) 2 h, (C) 3 h, and (D) 4 h at 600 °C in an N<sub>2</sub> atmosphere, respectively. (E) Schematic of the stepwise thermal decomposition to form N-CNTs.

basic units are catalyzed into N-CNTs on the nanocatalysts. Therefore, the similar to the bottom-up organic method [15,16,42], the formation process of N-CNTs involves the catalytic decomposition of ZIF-67 by N-Cdots, the formation of nanocatalysts and the growth of N-CNTs, respectively.

As previously mentioned, it is anticipated that the prepared N-CNTs may exhibit remarkable ORR electrocatalytic activities in rechargeable devices when used as fuel cells and metal-air batteries. Therefore, conventional three electrode cyclic voltammetry (CV) measurements

were conducted to evaluate the ORR catalytic activity. For the comparison, bare GCE, N-Cdots, Co–N–C nanohybrids and commercially available Pt/C catalysts were also tested under the same condition. As can be shown in Fig. 6(A) and Fig. S4 (Supporting Information), in addition to an inferior capacitive behavior, featureless peaks were observed for bare GCE (Curve a in Fig. S4A) in an N<sub>2</sub>-saturated solution. Although no noticeable feature was observed the same as before, a superior capacitive current with high conductivity was observed for N-Cdots (Curve a in Fig. S4B), Co–N–C nanohybrids (Curve a in Fig. S4C),

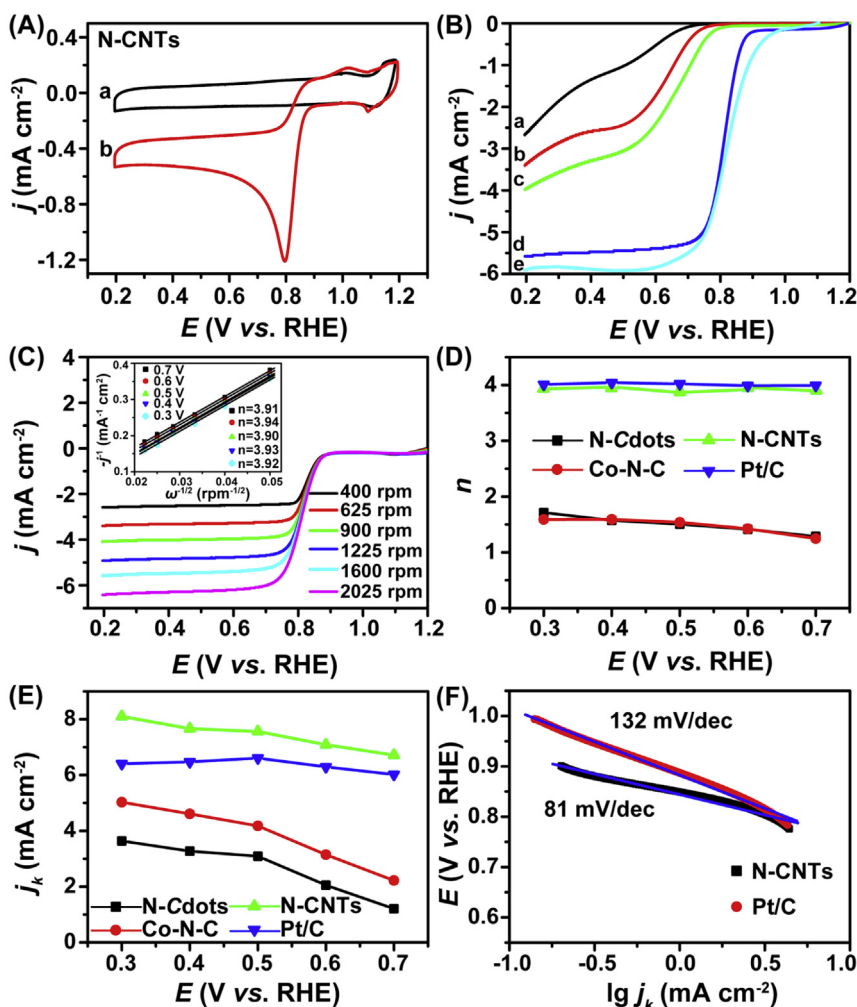


**Fig. 6.** (A) CVs for N-CNTs electrodes in  $N_2$ -saturated (curve a) and  $O_2$ -saturated (curve b) 0.1 M KOH at a scan rate of  $10 \text{ mV s}^{-1}$ . (B) LSVs for bare GCE (curve a), N-Cdots (curve b), Co-N-C nanohybrids (curve c), N-CNTs (curve d) and Pt/C electrodes (curve e) at 1600 rpm in  $O_2$ -saturated 0.1 M KOH with a scan rate of  $5 \text{ mV s}^{-1}$ . (C) LSVs of N-CNTs electrode in  $O_2$ -saturated 0.1 M KOH solution at a series of rotation rates from 400 to 2025 rpm with a scan rate of  $5 \text{ mV s}^{-1}$ , inset figure illustrates the  $K-L$  plots ( $j^{-1}$  versus  $\omega^{-1/2}$ ) of N-CNTs at different potentials. (D) Dependence of electron transfer number and (E) kinetic current density as the functions of potentials for N-Cdots, Co-N-C nanohybrids, N-CNTs and Pt/C electrode in  $O_2$ -saturated 0.1 M KOH, respectively. (F) Tafel plots of N-CNTs and Pt/C in  $O_2$ -saturated 0.1 M KOH where Tafel slopes were calculated by a linear regression method.

N-CNTs (Curve a in Fig. 6(A)) and Pt/C electrodes (Curve a in Fig. S4D) in an  $N_2$ -saturated solution. However, in the presence of  $O_2$ , a single cathodic oxygen reduction peak was observed for all cases, namely, 0.54 V for bare GCE (Curve b in Fig. S4A) and 0.65 V for N-Cdots (Curve b in Fig. S4B) and 0.73 V for Co-N-C nanohybrids (Curve b in Fig. S4C), respectively. However, the observed oxygen reduction peak of N-CNTs shifts to more positive potentials at 0.80 V (Curve b in Fig. 6(A)), which is an equivalent result to that of the commercially available Pt/C catalyst (0.83 V) (Curve b in Fig. S4D) for ORR. Moreover, the peak current density ( $j_p$ ) of N-CNTs ( $j_p = 1.21 \text{ mA/cm}^2$ ) is significantly (2 and 1.3 times) higher than the N-Cdots ( $j_p = 0.67 \text{ mA/cm}^2$ ) and Co-N-C nanohybrids ( $j_p = 0.95 \text{ mA/cm}^2$ ), respectively. Therefore, the more positive potentials and higher  $j_p$  explicitly suggest that the N-CNTs have an excellent catalytic activity for ORR. To further clarify the role of N-CNTs in ORR, linear sweep voltammetry (LSV) measurements were recorded on a rotating disk electrode (RDE) in an  $O_2$  saturated 0.1 M KOH electrolyte at a rotating rate of 1600 rpm. For the comparison, the ORR polarization plots of bare GCE, N-Cdots, Co-N-C nanohybrids and commercially available Pt/C electrodes were also obtained. As can be seen in Fig. 6(B), the onset potential ( $E_0 = 0.88 \text{ V}$ ) and half-wave potential ( $E_{1/2} = 0.82 \text{ V}$ ) of N-CNTs are remarkably more positive than those of GCE, N-Cdots and Co-N-C nanohybrids electrodes while they are only slightly negative than that of Pt/C catalyst ( $E_0 = 0.93 \text{ V}$ ,  $E_{1/2} = 0.83 \text{ V}$ ). Furthermore, the current density ( $j$ ) of N-CNTs ( $j = 5.58 \text{ mA/cm}^2$ ) is close to that of Pt/C ( $j = 5.89 \text{ mA/cm}^2$ ) and is higher than those of N-Cdots ( $j = 3.40 \text{ mA/cm}^2$ ) and Co-N-C nanohybrids ( $j = 3.98 \text{ mA/cm}^2$ ). These results are very consistent with CV measurements that N-CNTs possess highly efficient electrocatalytic

activity toward ORR. The fact that N-CNTs greatly outperformed N-Cdots and Co-N-C nanohybrids, which highlights the importance of the intimate contact between N-Cdots and Co-N-C nanohybrids toward an efficient charge transfer with respect to the ORR performance. Furthermore, to completely understand the electron transfer mechanism involved in the performance of ORR, the ORR polarization curves at different rotating speeds ( $\omega$ ) were discussed in detail. As shown in Fig. 6(C), Figs. S5(A), S5(C) and S5(E), the limiting current density ( $j_L$ ) increases with higher rotating rates for all catalysts because of the shortened diffusion length at higher speeds. These results are comparable to most of those previously reported for metal-free ORR catalysts and even for those recently reported on carbon-based catalysts with metals (Table S1) [42,43]. Moreover, in Fig. 6(C) inset, Figs. S5(B), S5(D) and S5(F), a linear relationship between the  $j^{-1}$  and  $\omega^{-1/2}$  has a similar slope to that of other studies in Koutecky–Levich ( $K-L$ ) plots, which indicates first-order reaction kinetics toward dissolved oxygen in the electrolyte solution [44]. It is well acknowledged that the four-electron ( $4e^-$ ) reduction pathway in an alkaline solution provides a faster oxygen reduction rate, which is beneficial for enhancing the charge and discharge properties of rechargeable devices. Therefore, the electron transfer number ( $n$ ) per oxygen molecule and the kinetic current density ( $j_k$ ) were analyzed thoroughly according to the  $K-L$  equations. In Fig. 6(D), values of  $n$  in the present study vary from 1.3 to 1.7 over the potential range for N-Cdots and Co-N-C nanohybrids, which show a two-electron ( $2e^-$ ) dominated ORR process with  $HO_2^-$  on the electrode. It is also well known that a two-step two-electron ( $2e^-$ ) dominates the ORR process, involving that the formation of intermediate species will decelerate the ORR processes. However, the N-

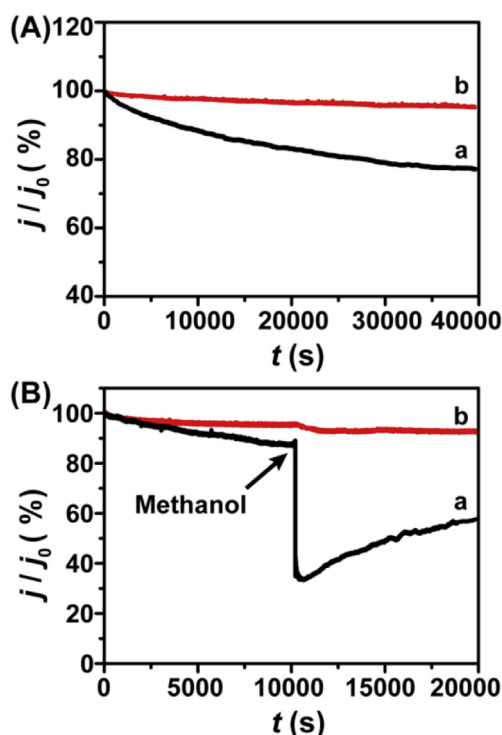


Fig. 7. (A) Chronoamperometry of N-CNTs and Pt/C electrodes in the  $O_2$ -saturated 0.1 M KOH solution at  $-0.40$  V for 40000 s ( $\sim 11$  h). (B) Chronoamperometric responses of N-CNTs and Pt/C electrodes in the 3 M methanol solution.

CNTs exhibit higher electron transfer numbers ( $\bar{n} = 3.92$ ) in potential ranges of 0.3–0.7 V, representing an efficient four-electron ( $4e^-$ ) dominated ORR process that is similar to that of the Pt/C catalyst ( $\bar{n} = 4.01$ ). As a result, the  $j_K$  value of N-CNTs can reach  $8.10 \text{ mA/cm}^2$  at 0.3 V, which is nearly 2.2 times larger than that of N-Cdots, 1.6 times larger than that of Co–N–C nanohybrids and 1.3 times larger than that of Pt/C as shown in Fig. 6(E), respectively. In addition, Tafel slope is an important element used to evaluate catalytic activity. As a result, the slope of N-CNTs being  $\sim 81 \text{ mV/dec}$  can be found to be much lower than that of the Pt/C catalyst ( $\sim 132 \text{ mV/dec}$ ) as shown in Fig. 6(F), which suggests that N-CNTs have faster kinetics. As a result, the  $4e^-$  ORR process reveals that N-CNTs provide superior electrocatalytic activity.

The commercially available Pt/C catalyst exhibits weak durability in relation to the ORR at the cathode in rechargeable devices. It is thus crucial to determine the stability and durability of the as-prepared catalyst. To shed light on this part, stability and durability are generally evaluated through chronoamperometric measurements at  $-0.4$  V for 40000 s ( $\sim 11$  h) for Pt/C and N-CNTs catalysts as shown in Fig. 7(A). Clearly, a slight loss in activity for the N-CNTs catalyst can be found (Curve b in Fig. 7(A)) whereas the Pt/C catalyst decreases nearly 22.9% of its initial activity (Curve a in Fig. 7(A)). These results indicate that the N-CNTs catalyst is much more stable than the commercial Pt/C in an alkaline solution. We further tested the methanol tolerance ability of N-CNTs and Pt/C catalysts by adding 3 M methanol with 10 mL in the 0.1 M KOH electrolyte (Fig. 7(B)). After adding methanol to the electrolyte, the current density of the Pt/C catalyst shows a sharp loss in activity of 45% (Curve a in Fig. 7(B)), whereas the N-CNTs retain a stable current response (Curve b in Fig. 7(B)). These results clearly show the superior catalytic tolerance of the N-CNTs catalyst and that it is more suitable for use as a cathode catalyst in alkaline fuel cells than the commercial Pt/C catalyst. Findings here not only provide a new insight into the preparation of N-CNTs, but also offer prospects of developing highly active ORR electrocatalysts in future rechargeable

devices.

#### 4. Conclusions

A direct pyrolysis with doping strategy was developed to prepare N-CNTs derived from N-Cdots and MOFs as a highly efficient electrocatalyst for ORR where N-Cdots serve as inducers of the graphitic structure and supply extra nitrogen, extending a potential electrocatalytic activity of N-CNTs. The SEM and TEM results indicate that N-Cdots, which have plenty of hydroxyl and amine groups, were able to catalyze the residual organic units and metal ions/clusters of ZIF-67 into thin N-CNTs with Co nanoparticles inside of them. The XPS and Raman spectra results suggest that N-Cdots serve as an inducer of the graphitic structure and an extra nitrogen supplier, which thus extends the potential electrocatalytic activity of N-CNTs. Results show that ZIF-67 in combination with N-Cdots generated a synergistic effect during the pyrolysis and carbonization processes, exhibiting a more highly efficient ORR electrocatalytic activity and durability than commercially available Pt/C in an alkaline solution. More importantly, the synthesis process of N-CNTs is simple, has a low energy consumption, and it could easily be employed in large-scale production. Therefore, the strategy developed here provides a new and general approach to the design of metal-free electrocatalysts for ORR.

#### Acknowledgments

This research was supported by National Natural Science Foundation of China (Grant No. 21175114) and a project founded by Lanzhou University of Technology. The research was also supported by the Ministry of Science and Technology through Grant No. 107-2923-E-007-002-MY3, 107-2112-M-007-030-MY3, 106-2923-E-007-006-MY2, 107-2119-M-009-019, 107-3017-F-007-002 and Y. L. Chueh greatly appreciates the use of the facility at CNMM.

#### Appendix A. Supplementary data

Supplementary data to this article can be found online at <https://doi.org/10.1016/j.nanoen.2019.05.074>.

#### References

- [1] O.Z. Sharaf, M.F. Orhan, An overview of fuel cell technology: Fundamentals and applications, *Renew. Sustain. Energy Rev.* 32 (2014) 810–853.
- [2] Y. Li, H. Dai, Recent advances in zinc-air batteries, *Chem. Soc. Rev.* 43 (2014) 5257–5275.
- [3] T. Cao, K. Huang, Y. Shi, N. Cai, Recent advances in high-temperature carbon-air fuel cells, *Energy Environ. Sci.* 10 (2017) 460–490.
- [4] C. Jiang, J. Ma, G. Corre, S.L. Jain, J.T.S. Irvine, Challenges in developing direct carbon fuel cells, *Chem. Soc. Rev.* 46 (2017) 2889–2912.
- [5] Z. Wang, D. Xu, J. Xu, X. Zhang, Oxygen electrocatalysts in metal-air batteries: from aqueous to nonaqueous electrolytes, *Chem. Soc. Rev.* 43 (2014) 7746–7786.
- [6] Y. Nie, L. Li, Z. Wei, Recent advancements in Pt and Pt-free catalysts for oxygen reduction reaction, *Chem. Soc. Rev.* 44 (2015) 2168–2201.
- [7] Z. Wen, J. Liu, J. Li, Core/Shell Pt/C Nanoparticles embedded in mesoporous carbon as a methanol-tolerant cathode catalyst in direct methanol fuel cells, *Adv. Mater.* 20 (2008) 743–747.
- [8] M. Shao, Q. Chang, J. Dodelet, R. Chenitz, Recent advances in electrocatalysts for oxygen reduction reaction, *Chem. Rev.* 116 (2016) 3594–3657.
- [9] K. Gong, F. Du, Z. Xia, M. Durstock, L. Dai, Nitrogen-doped carbon nanotube arrays with high electrocatalytic activity for oxygen reduction, *Science* 323 (2009) 760–764.
- [10] L. Feng, Y. Yan, Y. Chen, L. Wang, Nitrogen-doped carbon nanotubes as efficient and durable metal-free cathodic catalysts for oxygen reduction in microbial fuel cells, *Energy Environ. Sci.* 4 (2011) 1892–1899.
- [11] D. Yu, Q. Zhang, L. Dai, Highly efficient metal-free growth of nitrogen-doped single-walled carbon nanotubes on plasma-etched substrates for oxygen reduction, *J. Am. Chem. Soc.* 132 (2010) 15127–15129.
- [12] H.W. Zhu, C.L. Xu, D.H. Wu, B.Q. Wei, R. Vajtai, P.M. Ajayan, Direct synthesis of long single-walled carbon nanotube strands, *Science* 296 (2002) 884–886.
- [13] P.M. Ajayan, Nanotubes from carbon, *Chem. Rev.* 99 (1999) 1787–1800.
- [14] Y. Segawa, H. Ito, K. Itami, Structurally uniform and atomically precise carbon nanostructures, *Nat. Rev. Mater.* 1 (2016) 15002–15016.
- [15] S. Hitosugi, W. Nakanishi, T. Yamasaki, H. Isobe, Bottom-up synthesis of finite



- models of helical (n, m)-single-wall carbon nanotubes, *Nat. Commun.* 2 (2011) 492–496.
- [16] H. Omachi, Y. Segawa, K. Itami, Synthesis of cycloparaphenylenes and related carbon nanorings: a step toward the controlled synthesis of carbon nanotubes, *Acc. Chem. Res.* 45 (2012) 1378–1389.
- [17] P. Su, H. Xiao, J. Zhao, Y. Yao, Z. Shao, C. Li, Q. Yang, Nitrogen-doped carbon nanotubes derived from Zn-Fe-ZIF nanospheres and their application as efficient oxygen reduction electrocatalysts with in situ generated iron species, *Chem. Sci.* 4 (2013) 2941–2946.
- [18] B.Y. Xia, Y. Yan, N. Li, H.B. Wu, X. Lou, X. Wang, A metal-organic framework-derived bifunctional oxygen electrocatalyst, *Nat. Energy* 1 (2016) 15006–15013.
- [19] J. Meng, C. Niu, L. Xu, J. Li, X. Liu, X. Wang, Y. Wu, X. Xu, W. Chen, Q. Li, Z. Zhu, D. Zhao, L. Mai, General oriented formation of carbon nanotubes from metal-organic frameworks, *J. Am. Chem. Soc.* 139 (2017) 8212–8221.
- [20] H. Jin, H. Huang, Y. He, X. Feng, S. Wang, L. Dai, J. Wang, Graphene quantum dots supported by graphene nanoribbons with ultrahigh electrocatalytic performance for oxygen reduction, *J. Am. Chem. Soc.* 137 (2015) 7588–7591.
- [21] C. Hu, C. Yu, M. Li, X. Wang, Q. Dong, G. Wang, J. Qiu, Nitrogen-doped carbon dots decorated on graphene: a novel all-carbon hybrid electrocatalyst for enhanced oxygen reduction reaction, *Chem. Commun.* 51 (2015) 3419–3422.
- [22] S. Gao, Y. Chen, H. Fan, X. Wei, C. Hu, L. Wang, L. Qu, A green one-arrow-two-hawks strategy for nitrogen-doped carbon dots as fluorescent ink and oxygen reduction electrocatalysts, *J. Mater. Chem.* 2 (2014) 6320–6325.
- [23] C. Zhu, J. Zhai, S. Dong, Bifunctional fluorescent carbon nanodots: green synthesis via soy milk and application as metal-free electrocatalysts for oxygen reduction, *Chem. Commun.* 48 (2012) 9367–9369.
- [24] X. Yan, Y. Jia, X. Yao, Defects on carbons for electrocatalytic oxygen reduction, *Chem. Soc. Rev.* 47 (2018) 7628–7658.
- [25] W. Niu, R. Zhu, Y. Hua, H. Zeng, S. Cosnier, X. Zhang, D. Shan, One-pot synthesis of nitrogen-rich carbon dots decorated graphene oxide as metal-free electrocatalyst for oxygen reduction reaction, *Carbon* 109 (2016) 402–410.
- [26] T. Xing, Y. Zheng, L.H. Li, B.C.C. Cowie, D. Gunzelmann, S.Z. Qiao, S. Hang, Y. Chen, Observation of active sites for oxygen reduction reaction on nitrogen doped multilayer graphene, *ACS Nano* 8 (2014) 6856–6862.
- [27] X. Bai, Y. Shi, J. Guo, L. Gao, K. Wang, Y. Dua, T. Ma, Catalytic activities enhanced by abundant structural defects and balanced N distribution of N-doped graphene in oxygen reduction reaction, *J. Power Sources* 306 (2016) 85–91.
- [28] L. Shen, M. Chen, L. Hu, X. Chen, J. Wang, Growth and stabilization of silver nanoparticles on carbon dots and sensing application, *Langmuir* 29 (2013) 16135–16140.
- [29] L. Shen, Q. Chen, Z. Sun, X. Chen, J. Wang, Assay of biothiols by regulating the growth of silver nanoparticles with C-dots as reducing agent, *Anal. Chem.* 86 (2014) 5002–5008.
- [30] L. Zhang, W. Hou, Q. Lu, M. Liu, C. Chen, Y. Zhang, S. Yao, Colorimetric detection of hydrogen peroxide and lactate based on the etching of the carbon based Au-Ag bimetallic nanocomposite synthesized by carbon dots as the reductant and stabilizer, *Anal. Chim. Acta* 947 (2016) 23–31.
- [31] Y. Chen, C. Wang, Z. Wu, Y. Xiong, Q. Xu, S. Yu, H. Jiang, From bimetallic metal-organic framework to porous carbon: high surface area and multicomponent active dopants for excellent electrocatalysis, *Adv. Mater.* 27 (2015) 5010–5016.
- [32] W. Niu, D. Shan, R. Zhu, S. Deng, S. Cosnier, X. Zhang, Dumbbell-shaped carbon quantum dots/AuNCs nanohybrid as an efficient ratiometric fluorescent probe for sensing cadmium (II) ions and L-ascorbic acid, *Carbon* 96 (2016) 1034–1042.
- [33] K. Singh, F. Razmjooei, J. Yu, Active sites and factors influencing them for efficient oxygen reduction reaction in metal-N coordinated pyrolyzed and non-pyrolyzed catalysts: a review, *J. Mater. Chem.* 5 (2017) 20095–20119.
- [34] J.D. Wiggins-Camacho, K.J. Stevenson, Mechanistic discussion of the oxygen reduction reaction at nitrogen-doped carbon nanotubes, *J. Phys. Chem. C* 115 (2011) 20002–20010.
- [35] A. Kulkarni, S. Siahrostami, A. Patel, J.K. Nørskov, Understanding catalytic activity trends in the oxygen reduction reaction, *Chem. Rev.* 118 (2018) 2302–2312.
- [36] T. Wang, Z. Chen, Y. Chen, L. Yang, X. Yang, J. Ye, H. Xia, Z. Zhou, S. Sun, Identifying the active site of N-doped graphene for oxygen reduction by selective chemical modification, *ACS Energy Lett.* 3 (2018) 986–991.
- [37] A.C. Ferrari, D.M. Basko, Raman spectroscopy as a versatile tool for studying the properties of graphene, *Nat. Nanotechnol.* 8 (2013) 235–246.
- [38] J. Wu, M. Lin, X. Cong, H. Liu, P. Tan, Raman spectroscopy of graphene-based materials and its applications in related devices, *Chem. Soc. Rev.* 47 (2018) 1822–1873.
- [39] M. Kalbac, Y. Hsieh, H. Farhat, L. Kavan, M. Hofmann, J. Kong, M.S. Dresselhaus, Defects in individual semiconducting single wall carbon nanotubes: Raman spectroscopic and in situ Raman spectroelectrochemical study, *Nano Lett.* 10 (2010) 4619–4626.
- [40] Y. Jiang, L. Yang, T. Sun, J. Zhao, Z. Lyu, O. Zhuo, X. Wang, Q. Wu, J. Ma, Z. Hu, Significant contribution of intrinsic carbon defects to oxygen reduction activity, *ACS Catal.* 5 (2015) 6707–6712.
- [41] A. Eckmann, A. Felten, A. Mishchenko, L. Britnell, R. Krupke, K.S. Novoselov, C. Casiraghi, Probing the nature of defects in graphene by Raman spectroscopy, *Nano Lett.* 12 (2012) 3925–3930.
- [42] C. Xu, Q. Han, Y. Zhao, L. Wang, Y. Li, L. Qu, Sulfur-doped graphitic carbon nitride decorated with graphene quantum dots for an efficient metal-free electrocatalyst, *J. Mater. Chem.* 3 (2015) 1841–1846.
- [43] C.K. Chua, M. Pumera, Monothiolation and reduction of graphene oxide via one-pot synthesis: hybrid catalyst for oxygen reduction, *ACS Nano* 9 (2015) 4193–4199.
- [44] S. Dou, L. Tao, J. Huo, S. Wang, L. Dai, Etched and doped Co<sub>9</sub>S<sub>8</sub>/graphene hybrid for oxygen electrocatalysis, *Energy Environ. Sci.* 9 (2016) 1320–1326.



**Wen-Jun Niu** received his Ph.D. degree from the Institute of Environmental and Biological Engineering, Nanjing University of Science and Technology in 2017. Then, he joined Prof. Yu-Lun Chueh's group as a researcher at the State Key Laboratory of Advanced Processing and Recycling of Non-ferrous Metals, Lanzhou University of Technology. His current research interests focus on the development of carbon-based nanomaterials and their applications in energy conversion and storage, including water splitting, CO<sub>2</sub> reduction, oxygen reduction, and metal-air batteries.



**Ya-Ping Wang** is currently studying for degree of MS in State Key Laboratory of Advanced Processing and Recycling of Non-ferrous Metals, School of Materials Science and Engineering, Lanzhou University of Technology, Lanzhou 730050, PR China. Her research interests focus on the preparation of novel carbon materials and their applications in Rechargeable Zn-Air Batteries.



**Jin-Zhong He** is currently studying for degree of MS in State Key Laboratory of Advanced Processing and Recycling of Non-ferrous Metals, School of Materials Science and Engineering, Lanzhou University of Technology, Lanzhou 730050, PR China. His research interests focus on the electrocatalytic performance of carbon-related materials.



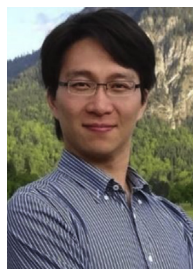
**Wen-Wu Liu** received his Ph.D. degree from the School of Metallurgical and Ecological Engineering, University of Science and Technology Beijing in 2017. Then, he joined the New Energy Materials team of Prof. Yu-Lun Chueh as a researcher at the State Key Laboratory of Advanced Processing and Recycling of Non-ferrous Metals, Lanzhou University of Technology. His current research interests focus on the development of organic-inorganic hybrid perovskite solar cells (PSCs), all inorganic PSCs, and the two-dimensional (2D) quantum dots materials and their applications in Lithium-sulfur battery and Sodium-ion battery.



**Mao-Cheng Liu** is an associate professor in School of Materials Science and Engineering, Lanzhou University of Technology, China. His research interests include (1) Development of binary metal oxides and metal phosphide/carbide alloys based pseudocapacitive materials and Na+ storage materials. (2) Fabrication of biomass-derived mesoporous carbon and high voltage electrical double layer capacitors.



**Dan Shan** is presently employed as a professor in School of Environmental and Biological Engineering, Nanjing University of Science & Technology, PR China. She received her MS in physical chemistry from Yangzhou University, China in 2001, and her Ph.D. in electrochemistry from Joseph Fourier University of Grenoble (France) in 2004. She worked at School of Chemistry & Chemical Engineering, Yangzhou University, PR China from 2004 to 2011. Her current fields of interest include biosensor, interfacial electrochemistry and electroconductive polymer.



**Yu-Lun Chueh** is a professor in Department of Materials Science and Engineering, National Tsing Hua University, Taiwan. His research directions include (1) Direct growth, fundamental characterizations, and optoelectronic applications of two-dimensional materials, including graphene and transition metal dichalcogenide. (2) Energy harvesting by Cu(In,Ga)Se<sub>2</sub> solar cells and phase-changed molten salts. (3) Low power resistive random access memory. Details can be found at: <http://nanoscienceandnanodevicelab.weebly.com/index.html>.



**Ling Lee** received his Ph.D. degree from Department of Electrophysics, National Chiao Tung University, Taiwan in 2008. Now he is a postdoctoral researcher in National Tsing Hua University, Taiwan. His research interests include the synthesis of low dimensional materials, the optical and electrical characterizations, and the discovery of crystallographic characteristics using synchrotron radiation.